

Structure of the archaeal chemotaxis protein CheY in a domain-swapped dimeric conformation

Karthik Shivaji Paithankar, Mathias Enderle, David C. Wirthensohn, Arthur Miller, Matthias Schlesner, Friedhelm Pfeiffer, Alexander Rittner, Martin Grininger, Dieter Oesterhelt

Angaben zur Veröffentlichung / Publication details:

Paithankar, Karthik Shivaji, Mathias Enderle, David C. Wirthensohn, Arthur Miller, Matthias Schlesner, Friedhelm Pfeiffer, Alexander Rittner, Martin Grininger, and Dieter Oesterhelt. 2019. "Structure of the archaeal chemotaxis protein CheY in a domain-swapped dimeric conformation." *Acta Crystallographica Section F - Structural Biology Communications* 75 (9): 576-85.
<https://doi.org/10.1107/s2053230x19010896>.



Structure of the archaeal chemotaxis protein CheY in a domain-swapped dimeric conformation

Karthik Shivaji Paithankar,^{a‡} Mathias Enderle,^{a‡} David C. Wirthensohn,^{b‡} Arthur Miller,^b Matthias Schlesner,^b Friedhelm Pfeiffer,^c Alexander Rittner,^a Martin Grininger^{a*} and Dieter Oesterhelt^{b*}

Received 23 April 2019
Accepted 4 August 2019

Edited by N. Sträter, University of Leipzig, Germany

‡ These authors contributed equally.

Keywords: chemotaxis; signal transduction; response regulator; CheY; CheF; archaeellum; protein evolution.

PDB references: PhCheY, 6er7; 6exr

Supporting information: this article has supporting information at journals.iucr.org/f

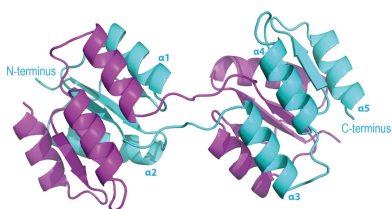
^aInstitute of Organic Chemistry and Chemical Biology, Buchmann Institute for Molecular Life Sciences, Goethe University Frankfurt, Max-von-Laue-Strasse 15, 60438 Frankfurt am Main, Germany, ^bDepartment of Membrane Biochemistry, Max Planck Institute of Biochemistry, Am Klopferspitz 18, 82152 Martinsried, Germany, and ^cComputational Biology Group, Max Planck Institute of Biochemistry, Am Klopferspitz 18, 82152 Martinsried, Germany. *Correspondence e-mail: grininger@chemie.uni-frankfurt.de, oesterhe@biochem.mpg.de

Archaea are motile by the rotation of the archaeellum. The archaeellum switches between clockwise and counterclockwise rotation, and movement along a chemical gradient is possible by modulation of the switching frequency. This modulation involves the response regulator CheY and the archaeellum adaptor protein CheF. In this study, two new crystal forms and protein structures of CheY are reported. In both crystal forms, CheY is arranged in a domain-swapped conformation. CheF, the protein bridging the chemotaxis signal transduction system and the motility apparatus, was recombinantly expressed, purified and subjected to X-ray data collection.

1. Introduction

Archaea and bacteria share the ability to move in response to chemical or physical stimuli towards favorable growth conditions (Marwan & Oesterhelt, 2000; Quax, Albers *et al.*, 2018). Motility is based on the rotation of the flagellum (in bacteria) and the archaeellum (in archaea; formerly known as the archaeal flagellum), respectively, and the directionality of the movement is provided by modulating the switching frequency in response to the stimulus (Armitage, 1999). The molecular basis underlying taxis is composed of two systems: chemotaxis signal transduction, which processes the external stimulus, and the flagellum/archaeellum, which responds to the chemotaxis output signal.

The Che proteins, encoded by genes that cluster in genomes, constitute the chemotaxis signal transduction system. The overall mechanism of chemotaxis is conserved in archaea and bacteria (Szurmant & Ordal, 2004). Receptors, generally known as methyl-accepting chemotaxis proteins (MCPs) and referred to as halobacterial transducer proteins (Htrs) in halophilic archaea (Zhang *et al.*, 1996), sense external stimuli such as chemicals, oxygen or light. The histidine kinase CheA and the response regulator CheY form a stimulus–response coupling mechanism, generally termed the two-component system (Parkinson & Kofoid, 1992; Parkinson, 1993). CheA autophosphorylates and subsequently donates the phosphate to CheY, yielding phosphorylated CheY (CheY-P; Garrity & Ordal, 1997; Bischoff *et al.*, 1993; Rudolph & Oesterhelt, 1995; Rudolph *et al.*, 1995). The concentration of CheY-P determines the switching frequency of the flagellum or archaeellum, respectively. Several Che proteins are involved in adapting (CheR, CheB, CheC, CheD and CheV; Springer & Koshland,



OPEN ACCESS

1977; Simms *et al.*, 1985, 1987; Stock & Koshland, 1978; Muff & Ordal, 2007; Karatan *et al.*, 2001; Schlesner *et al.*, 2012) or shutting down (CheZ, CheX, CheC and FliY; Silversmith, 2010; Sircar *et al.*, 2013) the response, the latter by removal of the phosphoryl modification from CheY-P.

In bacteria, CheY-P interacts with the flagellar motor switch protein FliM (Welch *et al.*, 1993). The CheY-P–FliM interaction has been shown to be responsible for increasing the probability of a switch in the rotational direction of the flagellum (Berg, 2003). In archaea, no homologs of FliM have been identified, and the interaction of CheY-P with different partners in bacteria and archaea has been considered to be a factor that separates the archaeal system of motility from the bacterial system of motility.

In interactomic studies, we have recently identified three candidate proteins in *Halobacterium salinarum* that are involved in the interaction of Che and Fla proteins (Schlesner *et al.*, 2009). Analysis of deletion strains provided compelling evidence that two open reading frames in particular, OE2401F and CheF1 (OE2402F), are essential for controlling the directionality of archaeellar rotation. OE2401F encodes a HEAT_PBS or HEAT family protein comprised of bihelical HEAT-like repeats. CheF1 encodes a protein from the conserved CheF-arch protein domain family (previously DUF439), which is exclusively found in Euryarchaea. *CheF* genes are consequently located in the chemotaxis gene regions and their occurrence is strictly correlated with the presence of *che* genes (Schlesner *et al.*, 2009, 2012). Protein–protein interaction analysis of the halobacterial Che proteins revealed that CheF1 directly interacts with CheY, CheD and CheC2, as well as with ArICE (FlaCE, OE_2386R). As such, CheF1 is proposed to provide the missing function of bridging the chemotaxis signal transduction system and the motility apparatus, thereby representing the factor that connects the Che cascade, which is shared by archaea and bacteria, to the archaea-specific motility apparatus. The archaeal CheY has recently been structurally determined and in its interplay with CheF has been analyzed, providing a basal molecular biological understanding of how a conserved chemotaxis system can target the entirely different motility structures in bacteria and archaea (Quax, Altegoer *et al.*, 2018). Here, we present single-crystal X-ray structures of CheY from *Pyrococcus horikoshii* (PhCheY) in two different crystal forms, and the protein purification, crystallization and X-ray data collection of CheF (PhCheF). Our data support the conservation of the bacterial and archaeal response-regulator proteins. We observe PhCheY to have a domain-swapped, pseudo-dimeric fold, which may reflect inherent properties of the protein fold but is not likely to be of physiological relevance.

2. Materials and methods

2.1. Macromolecule production

The coding sequences for PhCheF and PhCheY were provided by a synthetic plasmid carrying the ORFs PH0494 (PhCheF) and PH0482 (PhCheY) and were amplified by PCR

with PH0494 specific primers (forward primer AAGGAGA TATACATATGCCGATCTTTGAAGCCCCG; reverse primer GGTGGTGGTGCTCGAGCATGCTCACCAGGCCATATT TC) and PH0482 specific primers (forward primer AAG GAGATATACATATGGCTCGTGTCTGTTGT; reverse primer GGTGGTGGTGCTCGAGACTAGACAGCACACG GATTCAC). In an In-Fusion cloning reaction (Clontech, Japan), the gel-purified fragments were ligated with NdeI and XhoI linearized pET-22b(+) (Novagen, USA), yielding the plasmids pDW01-1 and pDW02-1 for the expression of PhCheF and PhCheY as C-terminally His-tagged proteins. For the construction of non-His-tagged variants, we removed the His tag by inserting TAG codons upstream of the XhoI restriction site via the site-directed mutagenesis method (plasmids pDW01-2 and pDW02-2).

For heterologous expression of proteins in *Escherichia coli*, the plasmids were transformed into BL21 Gold (DE3) cells (Agilent Technologies, USA). Single colonies were used to inoculate 35 ml LB medium containing 100 µg ml⁻¹ ampicillin and were incubated at 37°C for 16 h. This preculture was used to inoculate 2 l TB medium, which was grown at 37°C and 180 rev min⁻¹ until the mid-to-late log phase (OD₆₀₀ = 0.8–1.0) before inducing expression at 20°C with 0.5 mM IPTG. The cells were harvested after 16 h of protein expression, and the cell pellets were frozen in liquid nitrogen and stored at –80°C until further use. For purification, the cells were resuspended in appropriate buffers containing protease inhibitors (Roche, Switzerland) and DNaseI (Applichem, Germany) and were lysed using a French press. The lysates were centrifuged for 1 h at 4°C and 47 000g. After centrifugation, the supernatants were subjected to purification protocols. The non-His-tagged proteins PhCheF and PhCheY (in buffer H; 20 mM Tris–HCl pH 7.5, 100 mM NaCl, 5 mM DTT) were purified by heating the supernatant to 80°C for 20 min followed by centrifugation of the precipitated biomolecules at 24 000g for 20 min. As analyzed by SDS–PAGE, this treatment precipitated most of the proteins of the *E. coli* expression host, while the thermostable proteins PhCheF and PhCheY remained soluble. Concentration of PhCheF and PhCheY and size-exclusion chromatography (SEC) using a Superdex 200 26/60 column (GE Healthcare, USA), removing the remaining proteins and soluble biomolecules (as metabolites and nucleic acids), eventually yielded proteins that were suitable for biomolecular analysis and crystallization. His-tagged proteins were purified by nickel-chelating affinity chromatography [standard protocol; wash buffer W (20 mM Tris–HCl pH 7.5, 100 mM NaCl, 20 mM imidazole) and buffer E (the same as buffer W but with 500 mM imidazole)] and SEC (buffer H) using a Superdex 200 26/60 column (GE Healthcare, USA).

For the *in vitro* pull-down assay with PhCheF and His-tagged PhCheY, 2 ml of the supernatant of each preparation (after lysis using a French press and centrifugation) were first incubated at 37°C for 15 min (in buffer W with 20 mM imidazole). The incubated protein mixture was then added to 2.5 ml equilibrated Ni–NTA beads (in 5–7.5 ml buffer W). After further incubation at 4°C for 1 h, the slurry was

Table 1

Macromolecule-production information.

Sequences of PhCheF and PhCheY are available from UniProt with accession codes O58230 and O58193, respectively.

	PhCheF	PhCheY
Source organism	<i>P. horikoshii</i>	<i>P. horikoshii</i>
DNA source	Genomic DNA	Genomic DNA
Forward primer	AAGGAGATATACATATGCCGATCTTTGAAGCCCG	AAGGAGATATACATATGGCTCGTGTCTGGTTGT
Reverse primer	GGTGGTGGTGCCTCGAGCATGCTCACCAGGCCATATTTT	GGTGGTGGTGCCTCGAGACTAGACAGCACACGATTAC
Expression vector	pET-22b(+)	pET-22b(+)
Expression host	<i>E. coli</i>	<i>E. coli</i>
Complete amino-acid sequence of the construct produced	MPIFEARVKVGISSSVWTSRKSWSRDAIAQIESDRIVVKYLKMG GEVVGEDSFPSALIDLGVRIPELKLNPEKDHFGIKFYIP GRGELLVIFTIEENLLIYDEKKFSEFVHKVFEVLINGKTVM LQLARIIGGAVNMESKWEGLRVIKVKARSARTQKTERSTIVV IIKDKRPVSI FSDLEDIEIEEVDMMNGKRVRAWKIRHFHIDQ SVTSYLYIPDKQTQLYVLRLLKYNPAIMEFIMKVSDDFPT LKSEFQEI MEKEIKELEALDEMEKQIILVALYSGINPLELHQ FLGVSEKEIEEYDRMIDKGLLKIVMIRKIVDLTNEGRKIV NKLLKYGLVSM	MARVLVVDDAAFMRMLLKKILTQAGHEVVGEEASNGKEAVEKYK QLKPDLVMTDIVMPMDGITAVKEIMKIDPNAKIMITAVG QEAKVMEALKSGAKGYIVKPFQAQKVIIEVNRVLSS

Table 2

Crystallization.

	PhCheF	PhCheY
Method	Vapor diffusion, hanging drop	Vapor diffusion, hanging drop
Plate type	24-well plate	24-well plate
Temperature (K)	295	295
Protein concentration (mg ml ⁻¹)	10	10
Buffer composition of protein solution	20 mM Tris-HCl pH 7.5, 100 mM NaCl, 5 mM DTT	20 mM Tris-HCl pH 7.5, 100 mM NaCl
Composition of reservoir solution	0.1 M Tris-HCl pH 7.8, 0.1 M ammonium sulfate, 0.3 M sodium formate, 3% PGA-LM, 3% PEG 8000	0.1 M Tris-HCl pH 8.0, 1.2 M sodium malonate
Volume and ratio of drop	1:1	1:1
Volume of reservoir (μl)	750	750

subjected to a gravity-flow column. The beads were washed five times with buffer W (one column volume per step) and the proteins were eluted with buffer E (half a column volume per step). Fractions were collected and loaded onto a gel. The elution peak fractions were also subjected to SEC using a Superdex 200 10/300 column (GE Healthcare, USA). Ni-NTA pull-downs were also performed with 5 mM BeSO₄ as well as 50 mM NaF in the respective buffers to obtain the BeF₃⁻ species mimicking phosphorylated PhCheY (Lee *et al.*, 2001). Macromolecule-production information is summarized in Table 1.

2.2. Crystallization

PhCheF and PhCheY were screened using commercially available screens in 96-well plates. For crystallization, pooled fractions from SEC were used. PhCheF crystallized in 0.1 M Tris-HCl pH 7.8, 0.1 M ammonium sulfate, 0.3 M sodium formate, 3% PGA-LM, 3% PEG 8000. His-tagged PhCheY crystallized in 0.1 M Tris-HCl pH 8.0, 1.2 M sodium malonate. Crystallization information is summarized in Table 2.

2.3. Data collection and processing

Multi-wavelength anomalous dispersion (MAD) data for PhCheF were collected on beamline PX2 at the Swiss Light Source synchrotron facility, Villigen, Switzerland. The MAD data set was collected at three wavelengths: 0.9795 Å (peak),

0.9797 Å (inflection) and 0.9718 Å (remote). For this experiment, the crystal in the droplet was transferred into a cryo-solution consisting of the mother liquor supplemented with 20% (v/v) ethylene glycol for 1 min and was then cryocooled by plunging it into liquid nitrogen. X-ray diffraction data were recorded on a PILATUS 6M detector (Dectris) while the crystal was held in a gaseous N₂ stream at 100 K.

In the case of PhCheY, data sets were collected on beamline ID14-1 at the European Synchrotron Radiation Facility, Grenoble. The crystals were also maintained at 100 K, while data were recorded on a CCD detector (ADSC Quantum Q315r). All data sets were auto-processed and merged with the *xia2* suite (Winter *et al.*, 2013) using *XDS* (Kabsch, 2010) and *AIMLESS* (Evans & Murshudov, 2013). Data-collection and processing statistics are summarized in Table 3.

2.4. Structure solution and refinement

In the case of PhCheY, two different crystal forms were obtained in the monoclinic systems *P2* and *C2*. The solvent-content calculations for the *P2* crystal form performed with *MATTHEWS_COEF* (Matthews, 1968) indicated a solvent content of 58% with three molecules in the asymmetric unit. In the case of the *C2* crystal form, *MATTHEWS_COEF* indicated a solvent content of 57% with six molecules in the asymmetric unit. A search for the PhCheY sequence (UniProt accession code O58193) against the Protein Data Bank (PDB) with *BLAST* (Altschul *et al.*, 1990) revealed 71% sequence

Table 3
Data collection and processing.

Values in parentheses are for the outer shell. All data were processed to a $CC_{1/2}$ of 0.5.

	PhCheF, peak	PhCheF, inflection	PhCheF, remote	PhCheY	PhCheY
Diffraction source	SLS	SLS	SLS	ESRF	ESRF
Wavelength (Å)	0.9795	0.9797	0.9718	0.9334	0.9334
Temperature (K)	100	100	100	100	100
Detector	PILATUS 6M	PILATUS 6M	PILATUS 6M	ADSC Quantum Q315r	ADSC Quantum Q315r
Rotation range per image (°)	0.25	0.25	0.25	1	1
Total rotation range (°)	360	360	360	360	360
Exposure time per image (s)	0.25	0.25	0.25	5	5
Space group	$P2_1$	$P2_1$	$P2_1$	$P2$	$C2$
a, b, c (Å)	50.7, 188.7, 58.3	50.7, 188.7, 58.3	50.7, 188.7, 58.3	53.2, 65.7, 72.9	109.14, 124.38, 73.42
α, β, γ (°)	90, 113, 90	90, 113, 90	90, 113, 90	90, 111, 90	90, 112, 90
Resolution range (Å)	68.2–2.9 (3.0–2.9)	68.2–2.9 (3.0–2.9)	68.2–2.9 (3.0–2.9)	34–2.6 (2.7–2.6)	50–2.16 (2.20–2.16)
Total No. of reflections	278224	140306	151483	107515	355436
No. of unique reflections	21344	20363	21847	14172	11154
Completeness (%)	100 (100)	100 (100)	100 (100)	100 (99)	100 (99)
Multiplicity	7 (7)	7 (7)	7 (7)	7 (7)	7 (5)
$\langle I/\sigma(I) \rangle$	28 (3.6)	22 (2)	23 (2.5)	38 (3)	22 (1.2)†
$R_{p.i.m.}$	0.02 (0.8)	0.03 (0.3)	0.03 (0.5)	0.01 (0.4)	0.02 (0.6)
R_{meas}	0.06 (0.8)	0.06 (0.9)	0.06 (0.9)	0.03 (0.8)	0.02 (1.6)
Overall B factor from Wilson plot (Å ²)	86	91	88	68	41

† $\langle I/\sigma(I) \rangle$ is 2.0 at a resolution of 2.24 Å.

identity to *Thermotoga maritima* CheY (PDB entry 1u0s; Park *et al.*, 2004). Both PhCheY data sets were solved by the molecular-replacement method with *Phaser* (McCoy *et al.*, 2007) using a single chain of the structure with PDB code 1u0s. The resulting molecular-replacement models were refined with *REFMAC* (Murshudov *et al.*, 2011) with iterative manual model building with *Coot* (Emsley & Cowtan, 2004). Refinement statistics are summarized in Table 4. The PhCheF data could not be phased and therefore the structure could not be determined.

All structural figures were drawn using *PyMOL* (DeLano, 2002; <http://www.pymol.org>). Atomic coordinates and experimental structure factors for PhCheY in space groups $P2$ and $C2$ have been deposited in the PDB with accession codes 6er7 and 6exr, respectively. Raw X-ray diffraction data for both PhCheF and PhCheY are available from the Zenodo science data archive (<https://doi.org/10.5281/zenodo.1148967>).

3. Results and discussion

3.1. Preparation of *P. horikoshii* CheF and CheY

Proteins from *H. salinarum* have been expressed recombinantly in *E. coli*, but primarily as unfolded proteins that rely on the uncertainty of refolding protocols (Marg *et al.*, 2005; Grininger *et al.*, 2006). Therefore, we decided to work with CheF and CheY from *P. horikoshii* (termed PhCheF and PhCheY, respectively), which display sequence identities of 24 and 53% to CheF1 and CheY from *H. salinarum*, respectively (Supplementary Fig. S1). In addition, we expected increased thermostability of these proteins (Szilágyi & Závodszy, 2000) owing to the thermophilic lifestyle of the source (*P. horikoshii*; Kawarabayasi *et al.*, 1998).

3.2. Crystal structure of *P. horikoshii* CheY (PhCheY)

Three-dimensional structures of CheY from several organisms have been determined, for example those from

Table 4
Structure refinement for CheY.

Values in parentheses are for the outer shell.

	$P2$	$C2$
Resolution range (Å)	34–2.6 (2.70–2.60)	50–2.2 (2.20–2.16)
R_{cryst}/R_{free}	0.21/0.26	0.24/0.27
No. of non-H atoms	2688	11114
Protein residues in the asymmetric unit	351	698
R.m.s. deviations		
Bonds (Å)	0.01	0.01
Angles (°)	1.6	1.8
Average B factors (Å ²)		
Protein	92	54
Ramachandran plot		
Favored regions (%)	98.5	99.12
Allowed regions (%)	1.5	0.88
Outliers (%)	0	0

E. coli (Volz & Matsumura, 1991; Lee *et al.*, 2001), *Salmonella enterica* (Guhaniyogi *et al.*, 2006), *Thermotoga maritima* (Usher *et al.*, 1998), *Vibrio cholerae* (Biswas *et al.*, 2013) and *Helicobacter pylori* (Lam *et al.*, 2010). We aimed at determining the X-ray structure of PhCheY owing to the limited structural information on archaeal CheY [the crystal structure of a CheY-like protein from *Methanospirillum hungatei* JF-1 (PDB entry 3cg4; 31% sequence identity to PhCheY), the NMR structure of the CheY-like MTH538 from *Methanobacterium thermoautotrophicum* (PDB entry 1eiw; 31% sequence identity; Cort *et al.*, 2000) and the recent crystal structure from *Methanococcus maripaludis* (PDB entries 6ekg and 6ekh; 50% sequence identity; Quax, Altegoer *et al.*, 2018)].

The structures of CheY available in the PDB typically display a compact folded structural appearance. The subunits of CheY consistently show a $\beta 1/\alpha 1/\beta 2/\alpha 2/\beta 3/\alpha 3/\beta 4/\alpha 4/\beta 5/\alpha 5$ globular fold of five helices flanking a five-stranded parallel β -sheet. The subdomain in the N-terminal region (referred to

as the N-terminal domain; residues 1–53) has α -helices $\alpha 1$ – $\alpha 2$ packing on opposite sides of β -strands $\beta 1$ – $\beta 3$, and the C-terminal region of the molecule (referred to as the C-terminal domain; residues 61–118) has α -helices $\alpha 3$ – $\alpha 5$ packing against β -strands $\beta 3$ – $\beta 5$. In striking contrast to all of the known CheY structures, PhCheY adopts an open conformation in both crystal forms, with the two subdomains of a given subunit directed away from one another. In both of the two PhCheY structures solved in this study, two polypeptide chains assemble by pairing the N-terminal subdomain of a chain with the C-terminal subdomain of the other chain; *i.e.* the $\alpha 3/\beta 4/\alpha 4/\beta 5/\alpha 5$ part of the fold of each subunit packs with the $\beta 1/\alpha 1/\beta 2/\alpha 2$ part of the other subunit [Fig. 1(a)].

The crystal form with space group *P2* contains three non-crystallographic symmetry (NCS) molecules in the asymmetric unit. Superposition of the three subunits shows differing orientations between the domains, leading to an inter-domain movement of up to 90° [Fig. 1(b)]. The N- and C-terminal domains of PhCheY superimpose well onto each other in the crystal structure. The closest structural homolog is CheY from *T. maritima* (Usher *et al.*, 1998; PDB entry 1tmy; 71% sequence identity, with an r.m.s.d. of around 0.7 \AA and a Z-score of 25; Holm & Laakso, 2016). *T. maritima* CheY and PhCheY superimpose well, with the main deviation in the connecting region composed of the short helical segment of the $\beta 3$ – $\alpha 3$ loop. This region is unwound in the PhCheY

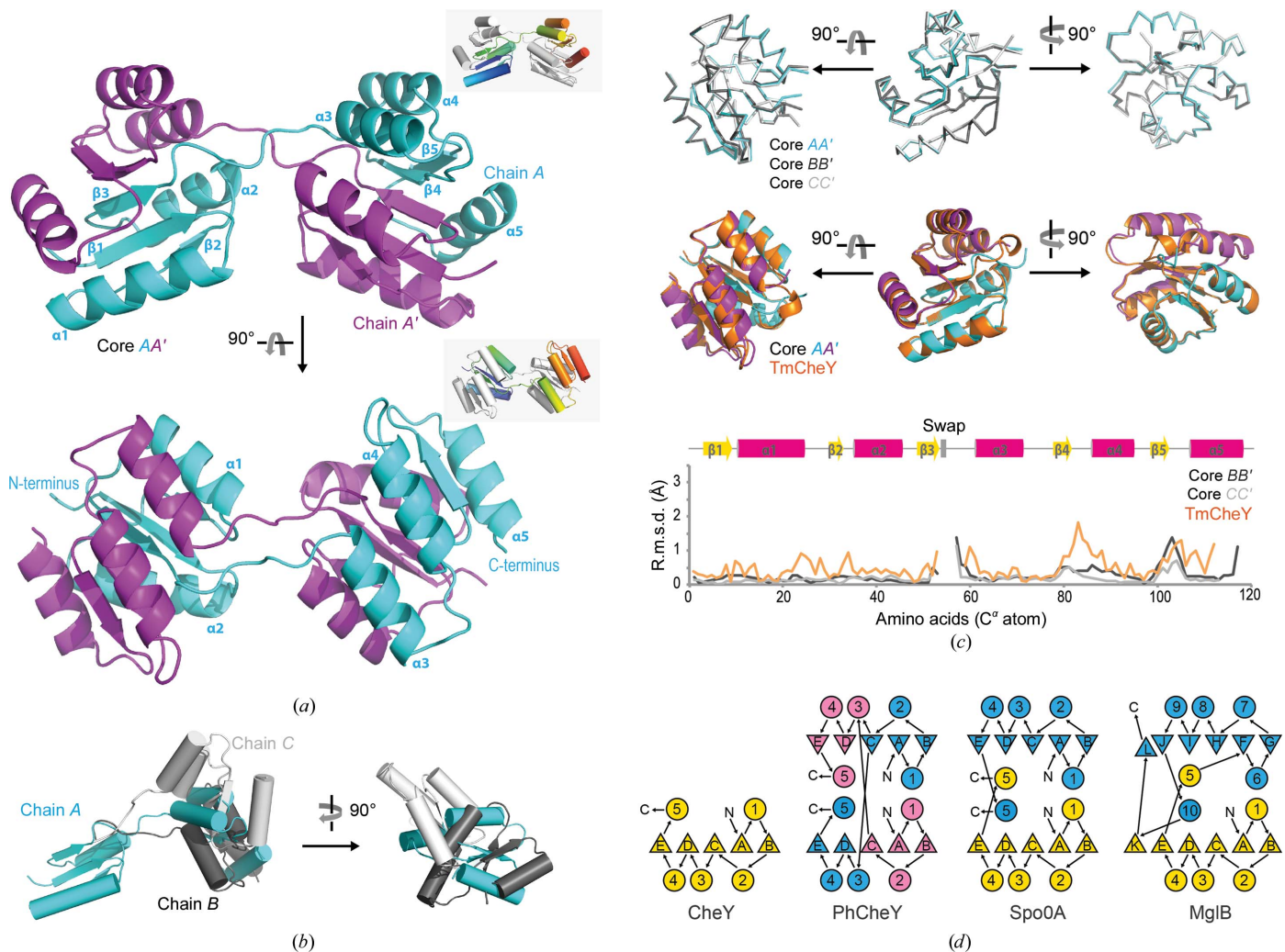


Figure 1
 Data for the crystal form in space group *P2* are shown. (a) Overall structure of PhCheY with the protomers of a dimeric structure colored cyan and magenta. PhCheY retains the overall $(\beta/\alpha)_5$ fold of CheY, but shows a different packing by swapping about half of the fold. Three molecules are found in the asymmetric unit. Chain *A* is shown in cyan and the symmetry-related chain *A'* is in magenta. The chains form a total interface of 2610 \AA^2 for the *AA'* interaction (the values are 2460 \AA^2 for the *BB'* interaction and 2420 \AA^2 for the *CC'* interaction). (b) Superposition of the polypeptide chains within the asymmetric unit. The N-terminal parts of the chains (residues 1–53) have been superimposed. Superpositions were calculated with the *LSQ* tool (least-squares fit) in *Coot* (Emsley *et al.*, 2010). (c) Superposition of PhCheY monomers (top; ribbon representation of backbone) and of a PhCheY pseudomonomer (reconstituted from chains *A* and *A'*) with *T. maritima* CheY (middle; PDB entry 1tmy; Usher *et al.*, 1998). R.m.s.d. plot showing deviations from a chain *A/A'* PhCheY pseudomonomer (bottom). Values were calculated with the *SSM* (secondary-structure match) tool in *Coot* (Emsley *et al.*, 2010). The r.m.s.d. diagram shows the largest overall deviation in the $\beta 3$ – $\alpha 3$ loop hinge region (values exceeding 3 \AA) as well as in the $\beta 5$ – $\alpha 5$ loop. (d) Topology diagram in the style of Fukami-Kobayashi *et al.* (1999) of the folds of CheY, the CheY homolog Spo0A and the evolutionarily related MglA.

structure (residues 54–60) [Fig. 1(c)], facilitating the inter-domain movement.

In the case of the *C2* crystal form, there are six molecules in the asymmetric unit. Four of the subunits (*A*, *B*, *D* and *F*) interact with one another in a dimeric-type domain-swapped assembly as described above. The other two subunits, *C* and *E*, interact with their own crystallographic symmetric molecules for the dimeric assembly with swapped domains. Superposition of the N-terminal subdomain among the different subunits *A*, *B*, *C*, *D*, *E* and *F* reveals that the C-terminal domain of subunits *B*, *C*, *D*, *E* and *F* undergoes a relative movement of up to 57° with respect to the N-terminal domain. In all cases, the rotational movement of the C-terminal domain was calculated after the initial superposition of the N-terminal domain. The connecting region between the $\beta 3$ – $\alpha 3$ loop is partially disordered for the two subunits *C* and *E*. For both crystal forms an unambiguous trace of the electron density in the $\beta 3$ – $\alpha 3$ loop was verified by a feature-enhanced map (FEM; Afonine *et al.*, 2015; shown in Supplementary Fig. S2 for the *P2* crystal form).

CheY has been discussed as the evolutionary ancestor fold of periplasmic binding proteins, such as for example the glucose/galactose-binding protein MglA. A domain swap, producing a pseudo-dimeric fold, has been suggested to be a key event in this process, and has been observed for the CheY-like protein Spo0A (Fukami-Kobayashi *et al.*, 1999; Lewis *et al.*, 2000) [Fig. 1(d)].

3.3. Comparison of archaeal CheY from *P. horikoshii* (PhCheY) and *M. maripaludis*

CheY from *M. maripaludis* has recently been structurally analyzed in the $\text{BeF}_3^-/\text{NaF}$ activated state, mimicking phosphorylation of the active aspartate Asp57 (Asp53 in PhCheY), and in the non-activated state (Quax, Altegoer *et al.*, 2018). The structural comparison revealed a repositioning of helix $\alpha 4$ accompanied by the displacement of the $\alpha 4$ – $\beta 4$ loop upon BeF_3^- binding, overall corresponding well to the structural changes that occur in *E. coli* and *T. maritima* CheY during activation (Lee *et al.*, 2001; Ahn *et al.*, 2013). The ‘back-swapped’ PhCheY pseudomonomer (reconstituted from chains *A* and *A'*) structure compares well with the structure of the non-activated CheY from *M. maripaludis* (r.m.s.d. of 1.1 Å, *Z*-score 22.1; Holm & Laakso, 2016) [Fig. 2(a)]. The positions of the active Asp53, as well as Thr81 and Tyr100, involved in translating the phosphorylation signal to a physiological output (Tyr–Thr coupling; Zhu *et al.*, 1996), also superimpose well, although Tyr100 adopts a different rotamer position [Fig. 2(b)]. The accumulated negative charge at the N-terminal region of helix $\alpha 4$ in *M. maripaludis* CheY has been suggested to provide an archaea-specific interface for CheF interaction (Quax, Altegoer *et al.*, 2018). As indicated by a qualitative surface-potential representation [Fig. 2(c)], PhCheY may be less negatively charged than *M. maripaludis* CheF, since it lacks a negatively charged amino acid at the position equivalent to Asp88 (Gly84 in PhCheY), as is also the case for other archaeal CheYs [Fig. 2(d)]. Glu91 is in a

different rotamer position in PhCheY and may also contribute to the less developed negative surface potential [see Fig. 2(c)].

3.4. Biochemical characterization of interactions of CheF and CheY

A difficult aspect in interaction studies of CheF and CheY is that CheY is supposed to interact with CheF in a phosphorylated state (CheY-P), which is however not accessible from recombinant expression. As a generally accepted treatment for mimicking phosphorylated states, we therefore incubated PhCheY with 5 mM BeSO_4 and 30 mM NaF to modify PhCheY with the phosphoryl analog BeF_3^- (Lee *et al.*, 2001). The elution profiles did not reveal higher apparent molecular masses when CheY and CheF were eluted together, indicating no complex formation [Fig. 3(a)]. While cross-linking with glutaraldehyde also failed in tracing interaction of the proteins under the selected conditions [Fig. 3(b)], an Ni-NTA pull-down assay eventually allowed the specific interaction of the proteins to be monitored by His-tagged PhCheY retaining PhCheF [Fig. 3(c)] during chromatographic elution. Both conditions, BeF_3^- -free and BeF_3^- -treated PhCheY, gave similar elution profiles. The complex observed in Ni-NTA pull-downs was not preserved during SEC. From Coomassie-stained SDS-PAGE in Ni-NTA pull-downs, PhCheY appears to be present in a molar excess, which might however result from nonsaturated PhCheY under the experimental conditions. We note that SEC showed the proteins to be monomeric after purification, with PhCheF having some tendency for the formation of a higher oligomeric species under the chosen conditions [see Fig. 3(a)]. Data collected during the biochemical characterization of CheY and CheF therefore do not support a physiological relevance of dimeric CheY species, as are observed in crystal structures.

4. Discussion

Two-component systems regulate a variety of fundamental processes in metabolism and motility, as well as a set of more specialized processes such as in virulence and development (Zschiedrich *et al.*, 2016). A prototypical response regulator is composed of two domains: a receiver domain and an output domain. The receiver domain operates in a highly conserved mode of accepting a phosphoryl modification from the histidine kinase and forwarding this information to an effector domain. The effector domain triggers the output response, and the variety of effector domains allows a large number of responses regulated by two-component signals (Gao & Stock, 2009).

Owing to its important role in signal transduction, CheY has been intensively studied in recent decades. CheY proteins have been characterized as standalone proteins, resting in an equilibrium of non-activated and activated states that is shifted in response to phosphorylation (Lowry *et al.*, 1994; Lee *et al.*, 2001; Gardino & Kern, 2007). CheY is consistently described as monomeric even at high concentrations and to be independent of the phosphorylation state. As the

phosphorylated state is inherently unstable, with half-lives from seconds to several hours under ambient conditions (Swanson *et al.*, 1996; Sanna *et al.*, 1995), analysis of the conformational state of activated CheY is complicated, however, and for structural studies phosphorylation was mainly just mimicked by using BeF_3^- -containing buffers (Lee *et al.*, 2001). In the current idea of a working mode for CheY, the activated state is read out by a subtly changed protein surface (Lee *et al.*, 2001; Gao & Stock, 2009; Quax, Altegoer *et al.*, 2018).

While CheY has been broadly characterized in structure and function, a subdomain swap, as observed in PhCheY, has not been reported before. However, it was found that the CheY α/β protein fold itself does allow domain swapping. Dimerization by domain swapping has been observed for the CheY-homologous sporulation response regulator Spo0A, although the physiological relevance of this structure was

questioned in this case owing to nonphysiological crystallization at low pH (Lewis *et al.*, 2000). Further, the pseudodimeric fold of periplasmic binding proteins such as MglB [see Fig. 1(d)] has been suggested to have evolved from a CheY-like ancestor protein by a domain swap (Fukami-Kobayashi *et al.*, 1999). When considering structural and conformational properties of the CheY fold, it is also informative to regard the folding properties of CheY. Studies on CheY revealed a heterogeneous folding trajectory, which is composed of N- and C-terminal subdomain folding in a hierarchical fashion with subdomain borders found swapped as in this study (Hills & Brooks, 2008, López-Hernández & Serrano, 1996). Both the structural properties of the CheY fold and the folding kinetics of CheY manifest the view of CheY being composed of two separate subdomains.

The assessment of the physiological relevance of the domain-swapped dimeric PhCheY is strongly connected to the

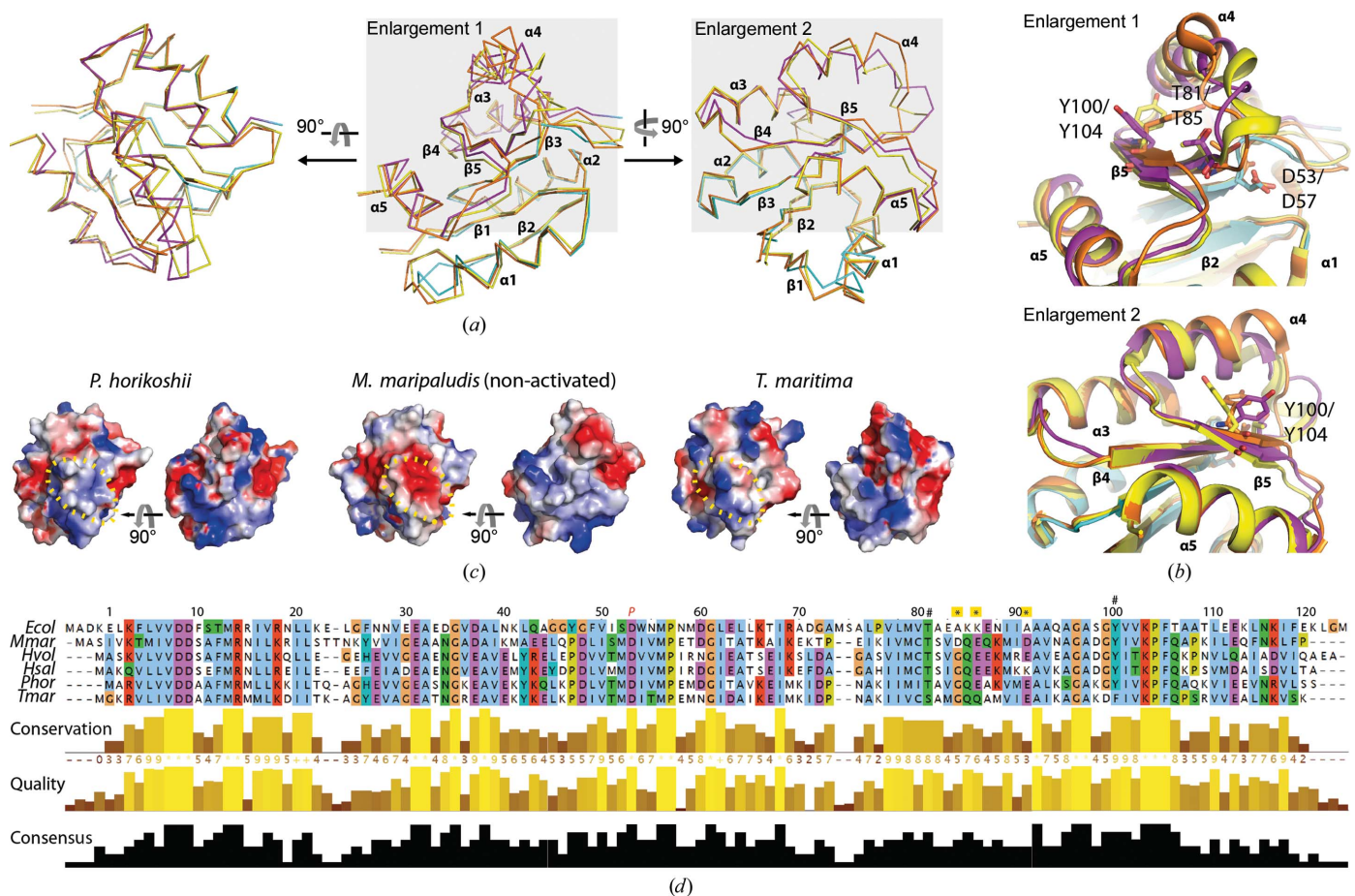
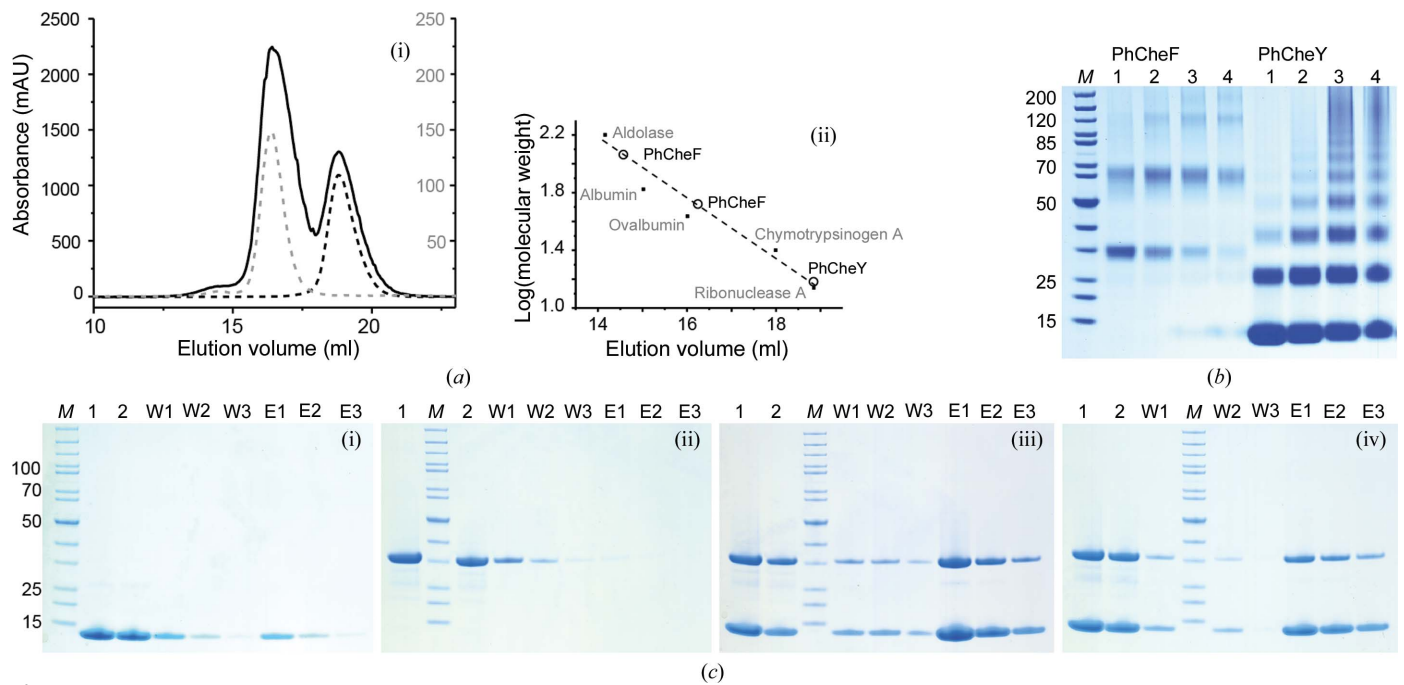


Figure 2 Comparative analysis of CheY. (a) Superposition of the PhCheY pseudomonomer (reconstituted from chains A and A') with *M. maripaludis* CheY (PDB entries 6ekg and 6ekh; Quax, Altegoer *et al.*, 2018). Views and arrangement are as in Fig. 1(c). Superpositions were calculated with the LSQ tool (least-squares fit) in Coot (Emsley *et al.*, 2010). PhCheY is in magenta/cyan and $\text{BeF}_3^-/\text{NaF}$ -activated and non-activated *M. maripaludis* CheY are in orange and yellow, respectively. The gray background refers to (b). (b) Enlargement of the CheY structures in the orientations indicated in (a). Residues Asp53/Asp57 (*P. horikoshii*/*M. maripaludis* numbering), Tyr100/Tyr104 and Thr81/Thr84 are shown in stick representation using the color code in (a). (c) Qualitative surface electrostatic representation of CheY from *P. horikoshii*, *M. maripaludis* and *T. maritima* (PDB entry 1tmy; Usher *et al.*, 1998) calculated with the vacuum electrostatics function in PyMOL (<http://www.pymol.org>) and shown in default coloring with positive potentials depicted in blue and negative potentials in red. The $\alpha4$ helices including the positions of Gln85 and Glu86 (*P. horikoshii* numbering; Glu89 and Gln90 in *M. maripaludis*) are circled in yellow. (d) Sequence alignment in *P. horikoshii* numbering generated with Clustal Omega (Thompson *et al.*, 1997) and rendered in Jalview (Waterhouse *et al.*, 2009).


Figure 3

Interaction studies using size-exclusion chromatography (SEC) and Ni-NTA pull-down. (a) (i) SEC profiles of PhCheF (39.7 kDa; gray dashed line), PhCheY (13.1 kDa; black dashed line) and a 1:1 stoichiometric mixture of proteins (black line). (ii) Calibration with ribonuclease (13.7 kDa), chymotrypsinogen A (25 kDa), ovalbumin (43 kDa), albumin (66.2 kDa) and aldolase (158 kDa). The peaks for PhCheY and PhCheF correspond to apparent molecular weights of 15 kDa and 41 and 127 kDa, respectively (calculated molecular weights of 13.1 and 39.7 kDa, respectively). The higher oligomeric species seen for PhCheF corresponds in its apparent molecular weight to a dimeric or trimeric complex. A mixture of PhCheF and PhCheY does not form complexes under the conditions of the experiment. (b) Coomassie-stained SDS-PAGE gel (NuPAGE, 4–12%, Invitrogen, USA) of cross-linking studies with glutaraldehyde. Samples 1–4 reflect different incubation times before quenching (1, 2, 5 and 10 min). For PhCheF, a pronounced dimeric species appears under moderate cross-linking conditions, while PhCheY seems to successively polymerize from monomers. The SDS-PAGE image was modified in contrast. (c) Coomassie-stained SDS-PAGE gel (NuPAGE, 4–12%, Invitrogen, USA) of the Ni-NTA pull-down assay with PhCheF and His-tagged PhCheY. Gels (i) and (ii) show controls with PhCheY and PhCheF, respectively; gels (iii) and (iv) show pull-down with nontreated (iii) and BeF₃⁻-treated (iv) PhCheY. PhCheF elutes with PhCheY in (iii) and (iv), suggesting specific interaction. Lane M, marker (PageRuler, unstained protein ladder; Thermo Scientific, USA); lane 1, control (samples incubated without Ni beads); lane 2, control (supernatant after incubation with Ni beads); lanes W1, W2 and W3, wash fractions; lanes E1, E2 and E3, elution fractions. The SDS-PAGE images were modified in contrast.

question of whether reversible domain swapping could occur on a time scale that is relevant for signaling. To switch between a monomeric and a dimeric state, an interface of roughly 1300 Å² between the subdomains of PhCheY would need to dissociate and reassociate in response to phosphorylation. Considering that the active aspartate (Asp53) is located in a positionally variable loop, it is unlikely that phosphorylation could efficiently induce the dissociation of the fold and enrich a ‘swapped’ form. Therefore, a physiological role for a domain-swapped dimeric PhCheY has to be ruled out. A physiological role of a domain-swapped dimer would also contradict the current understanding of the function of CheY (Quax, Altegoer *et al.*, 2018).

Crystallization of PhCheY as a domain-swapped dimer can rather be explained as follows: PhCheY is monomeric in solution, as suggested by SEC [see Fig. 3(a)], and in SDS-PAGE of cross-linking experiments [see Fig. 3(b)]. Owing to a putative cold-induced destabilization of PhCheY (*P. horikoshii* grows at 98°C), and putatively further induced by the crystallization conditions, the PhCheY fold disassembles into an open subdomain-dissociated conformation. At the high protein concentration in the crystallization drop, PhCheY can then reassemble from this open state with a partner poly-

peptide to form a domain-swapped dimeric assembly that is eventually removed from the monomer–dimer equilibrium by crystallization.

It is surely exciting to further reveal the different structural appearances of archaeal and bacterial CheY in order to disclose the principles of diversification in bacterial and archaeal chemotaxis/motility systems, which is then further pronounced by CheY interacting with FliM in bacteria and with CheF in archaea (Szurmant & Ordal, 2004; Albers & Jarrell, 2015; Schlesner *et al.*, 2009; Quax, Albers *et al.*, 2018).

5. Related literature

The following references are cited in the supporting information to this article: Albers & Jarrell (2018), Banerjee *et al.* (2013, 2015), Briegel *et al.* (2017), Buchan *et al.* (2013), Chaudhury *et al.* (2016, 2018), Cohen-Krausz & Trachtenberg (2002), Daum *et al.* (2017), Faguy *et al.* (1994), Frishman & Argos (1995), Gerl & Sumper (1988), Ghosh *et al.* (2011), Jarrell & McBride (2008), Kinoshita *et al.* (2016), Kupper *et al.* (1994), Meshcheryakov & Wolf (2016), Patenge *et al.* (2001), Peabody *et al.* (2003), Reindl *et al.* (2013), Speranskii *et al.* (1996), Streif *et al.* (2008) and Thomas & Jarrell (2001).

Acknowledgements

We thank the EMBL–ESRF Joint Structural Biology Group for help on the ESRF beamlines and the Swiss Light Source for beamtime. We are grateful to Andrei Lupas for support in the analysis of CheF structure and function, and to Ulrich Ermler and Andrew McCarthy for advice and help in processing the CheF data sets.

References

Afonine, P. V., Moriarty, N. W., Mustyakimov, M., Sobolev, O. V., Terwilliger, T. C., Turk, D., Urzhumtsev, A. & Adams, P. D. (2015). *Acta Cryst. D* **71**, 646–666.

Ahn, D.-R., Song, H., Kim, J., Lee, S. & Park, S. (2013). *Int. J. Biol. Macromol.* **54**, 76–83.

Albers, S. V. & Jarrell, K. F. (2015). *Front. Microbiol.* **6**, 23.

Albers, S. V. & Jarrell, K. F. (2018). *Trends Microbiol.* **26**, 351–362.

Altschul, S. F., Gish, W., Miller, W., Myers, E. W. & Lipman, D. J. (1990). *J. Mol. Biol.* **215**, 403–410.

Armitage, J. P. (1999). *Adv. Microb. Physiol.* **41**, 229–289.

Banerjee, A., Neiner, T., Tripp, P. & Albers, S. V. (2013). *FEBS J.* **280**, 6141–6149.

Banerjee, A., Tsai, C.-L., Chaudhury, P., Tripp, P., Arvai, A. S., Ishida, J. P., Tainer, J. A. & Albers, S.-V. (2015). *Structure*, **23**, 863–872.

Berg, H. C. (2003). *Annu. Rev. Biochem.* **72**, 19–54.

Bischoff, D. S., Bourret, R. B., Kirsch, M. L. & Ordal, G. W. (1993). *Biochemistry*, **32**, 9256–9261.

Biswas, M., Dey, S., Khamrui, S., Sen, U. & Dasgupta, J. (2013). *PLoS One*, **8**, e73923.

Briegel, A., Oikonomou, C. M., Chang, Y.-W., Kjaer, A., Huang, A. N., Kim, K. W., Ghosal, D., Nguyen, H. H., Kenny, D., Ogorzalek Loo, R. R., Gunsalus, R. P. & Jensen, G. J. (2017). *EMBO Rep.* **18**, 1660–1670.

Buchan, D. W. A., Minneci, F., Nugent, T. C. O., Bryson, K. & Jones, D. T. (2013). *Nucleic Acids Res.* **41**, W349–W357.

Chaudhury, P., Neiner, T., D’Imprima, E., Banerjee, A., Reindl, S., Ghosh, A., Arvai, A. S., Mills, D. J., van der Does, C., Tainer, J. A., Vonck, J. & Albers, S.-V. (2016). *Mol. Microbiol.* **99**, 674–685.

Chaudhury, P., van der Does, C. & Albers, S.-V. (2018). *PeerJ*, **6**, e4984.

Cohen-Krausz, S. & Trachtenberg, S. (2002). *J. Mol. Biol.* **321**, 383–395.

Cort, J. R., Yee, A., Edwards, A. M., Arrowsmith, C. H. & Kennedy, M. A. (2000). *J. Mol. Biol.* **302**, 189–203.

Daum, B., Vonck, J., Bellack, A., Chaudhury, P., Reichelt, R., Albers, S.-V., Rachel, R. & Kuhlbrandt, W. (2017). *Elife*, **6**, e27470.

DeLano, W. L. (2002). *CCP4 Newsl. Protein Crystallogr.* **40**, 11.

Emsley, P. & Cowtan, K. (2004). *Acta Cryst. D* **60**, 2126–2132.

Emsley, P., Lohkamp, B., Scott, W. G. & Cowtan, K. (2010). *Acta Cryst. D* **66**, 486–501.

Evans, P. R. & Murshudov, G. N. (2013). *Acta Cryst. D* **69**, 1204–1214.

Faguy, D. M., Jarrell, K. F., Kuzio, J. & Kalmokoff, M. L. (1994). *Can. J. Microbiol.* **40**, 67–71.

Frishman, D. & Argos, P. (1995). *Proteins*, **23**, 566–579.

Fukami-Kobayashi, K., Tateno, Y. & Nishikawa, K. (1999). *J. Mol. Biol.* **286**, 279–290.

Gao, R. & Stock, A. M. (2009). *Annu. Rev. Microbiol.* **63**, 133–154.

Gardino, A. K. & Kern, D. (2007). *Methods Enzymol.* **423**, 149–165.

Garrity, L. F. & Ordal, G. W. (1997). *Microbiology*, **143**, 2945–2951.

Gerl, L. & Sumper, M. (1988). *J. Biol. Chem.* **263**, 13246–13251.

Ghosh, A., Hartung, S., van der Does, C., Tainer, J. A. & Albers, S.-V. (2011). *Biochem. J.* **437**, 43–52.

Grininger, M., Zeth, K. & Oesterheld, D. (2006). *J. Mol. Biol.* **357**, 842–857.

Guhaniyogi, J., Robinson, V. L. & Stock, A. M. (2006). *J. Mol. Biol.* **359**, 624–645.

Hills, R. D. Jr & Brooks, C. L. (2008). *J. Mol. Biol.* **382**, 485–495.

Holm, L. & Laakso, L. M. (2016). *Nucleic Acids Res.* **44**, W351–W355.

Jarrell, K. F. & McBride, M. J. (2008). *Nature Rev. Microbiol.* **6**, 466–476.

Kabsch, W. (2010). *Acta Cryst. D* **66**, 125–132.

Karatan, E., Saulmon, M. M., Bunn, M. W. & Ordal, G. W. (2001). *J. Biol. Chem.* **276**, 43618–43626.

Kawarabayasi, Y., Sawada, M., Horikawa, H., Haikawa, Y., Hino, Y., Yamamoto, S., Sekine, M., Baba, S.-I., Kosugi, H., Hosoyama, A., Nagai, Y., Sakai, M., Ogura, K., Otsuka, R., Nakazawa, H., Takamiya, M., Ohfuku, Y., Funahashi, T., Tanaka, T., Kudoh, Y., Yamazaki, J., Kushida, N., Oguchi, A., Aoki, K.-I. & Kikuchi, H. (1998). *DNA Res.* **5**, 55–76.

Kinosita, Y., Uchida, N., Nakane, D. & Nishizaka, T. (2016). *Nature Microbiol.* **1**, 16148.

Kupper, J., Marwan, W., Typke, D., Grünberg, H., Uwer, U., Gluch, M. & Oesterheld, D. (1994). *J. Bacteriol.* **176**, 5184–5187.

Lam, K. H., Ling, T. K. W. & Au, S. W. (2010). *J. Bacteriol.* **192**, 2324–2334.

Lee, S.-Y., Cho, H. S., Pelton, J. G., Yan, D., Berry, E. A. & Wemmer, D. E. (2001). *J. Biol. Chem.* **276**, 16425–16431.

Lewis, R. J., Muchová, K., Brannigan, J. A., Barák, I., Leonard, G. & Wilkinson, A. J. (2000). *J. Mol. Biol.* **297**, 757–770.

López-Hernández, E. & Serrano, L. (1996). *Fold. Des.* **1**, 43–55.

Lowry, D. F., Roth, A. F., Rupert, P. B., Dahlquist, F. W., Moy, F. J., Domaille, P. J. & Matsumura, P. (1994). *J. Biol. Chem.* **269**, 26358–26362.

Marg, B. L., Schweimer, K., Sticht, H. & Oesterheld, D. (2005). *Biochemistry*, **44**, 29–39.

Marwan, W. & Oesterheld, D. (2000). *ASM News*, **66**, 83–89.

Matthews, B. W. (1968). *J. Mol. Biol.* **33**, 491–497.

McCoy, A. J., Grosse-Kunstleve, R. W., Adams, P. D., Winn, M. D., Storoni, L. C. & Read, R. J. (2007). *J. Appl. Cryst.* **40**, 658–674.

Meshcheryakov, V. A. & Wolf, M. (2016). *Protein Sci.* **25**, 1147–1155.

Muff, T. J. & Ordal, G. W. (2007). *J. Biol. Chem.* **282**, 34120–34128.

Murshudov, G. N., Skubák, P., Lebedev, A. A., Pannu, N. S., Steiner, R. A., Nicholls, R. A., Winn, M. D., Long, F. & Vagin, A. A. (2011). *Acta Cryst. D* **67**, 355–367.

Park, S.-Y., Beel, B. D., Simon, M. I., Bilwes, A. M. & Crane, B. R. (2004). *Proc. Natl Acad. Sci. USA*, **101**, 11646–11651.

Parkinson, J. S. (1993). *Cell*, **73**, 857–871.

Parkinson, J. S. & Kofoed, E. C. (1992). *Annu. Rev. Genet.* **26**, 71–112.

Patenge, N., Berendes, A., Engelhardt, H., Schuster, S. C. & Oesterheld, D. (2001). *Mol. Microbiol.* **41**, 653–663.

Peabody, C. R., Chung, Y. J., Yen, M.-R., Vidal-Ingigliardi, D., Pugsley, A. P. & Saier, M. H. Jr (2003). *Microbiology*, **149**, 3051–3072.

Quax, T. E. F., Albers, S.-V. & Pfeiffer, F. (2018). *Emerg. Top. Life Sci.* **2**, 535–546.

Quax, T. E. F., Altegoer, F., Rossi, F., Li, Z., Rodriguez-Franco, M., Kraus, F., Bange, G. & Albers, S.-V. (2018). *Proc. Natl Acad. Sci. USA*, **115**, E1259–E1268.

Reindl, S., Ghosh, A., Williams, G. J., Lassak, K., Neiner, T., Henche, A. L., Albers, S.-V. & Tainer, J. A. (2013). *Mol. Cell*, **49**, 1069–1082.

Rudolph, J. & Oesterheld, D. (1995). *EMBO J.* **14**, 667–673.

Rudolph, J., Tolliday, N., Schmitt, C., Schuster, S. C. & Oesterheld, D. (1995). *EMBO J.* **14**, 4249–4257.

Sanna, M. G., Swanson, R. V., Bourret, R. B. & Simon, M. I. (1995). *Mol. Microbiol.* **15**, 1069–1079.

Schlesner, M., Miller, A., Besir, H., Aivaliotis, M., Streif, J., Scheffer, B., Siedler, F. & Oesterheld, D. (2012). *BMC Microbiol.* **12**, 272.

Schlesner, M., Miller, A., Streif, S., Staudinger, W. F., Müller, J., Scheffer, B., Siedler, F. & Oesterheld, D. (2009). *BMC Microbiol.* **9**, 56.

Silversmith, R. E. (2010). *Curr. Opin. Microbiol.* **13**, 177–183.

Simms, S. A., Keane, M. G. & Stock, J. (1985). *J. Biol. Chem.* **260**, 10161–10168.

- Simms, S. A., Stock, A. M. & Stock, J. B. (1987). *J. Biol. Chem.* **262**, 8537–8543.
- Sircar, R., Greenswag, A. R., Bilwes, A. M., Gonzalez-Bonet, G. & Crane, B. R. (2013). *J. Biol. Chem.* **288**, 13493–13502.
- Speranskii, V. V., Metlina, A. L., Novikova, T. M. & Bakeyeva, L. Y. (1996). *Biophysics*, **41**, 167–173.
- Springer, W. R. & Koshland, D. E. Jr (1977). *Proc. Natl Acad. Sci. USA*, **74**, 533–537.
- Stock, J. B. & Koshland, D. E. Jr (1978). *Proc. Natl Acad. Sci. USA*, **75**, 3659–3663.
- Streif, S., Staudinger, W. F., Marwan, W. & Oesterhelt, D. (2008). *J. Mol. Biol.* **384**, 1–8.
- Swanson, R. V., Sanna, M. G. & Simon, M. I. (1996). *J. Bacteriol.* **178**, 484–489.
- Szilágyi, A. & Závodszy, P. (2000). *Structure*, **8**, 493–504.
- Szurmant, H. & Ordal, G. W. (2004). *Microbiol. Mol. Biol. Rev.* **68**, 301–319.
- Thomas, N. A. & Jarrell, K. F. (2001). *J. Bacteriol.* **183**, 7154–7164.
- Thompson, J. D., Gibson, T. J., Plewniak, F., Jeanmougin, F. & Higgins, D. G. (1997). *Nucleic Acids Res.* **25**, 4876–4882.
- Usher, K. C., De La Cruz, A. F., Dahlquist, F. W., Remington, S. J., Swanson, R. V. & Simon, M. I. (1998). *Protein Sci.* **7**, 403–412.
- Volz, K. & Matsumura, P. (1991). *J. Biol. Chem.* **266**, 15511–15519.
- Waterhouse, A. M., Procter, J. B., Martin, D. M., Clamp, M. & Barton, G. J. (2009). *Bioinformatics*, **25**, 1189–1191.
- Welch, M., Oosawa, K., Aizawa, S. & Eisenbach, M. (1993). *Proc. Natl Acad. Sci. USA*, **90**, 8787–8791.
- Winter, G., Lobley, C. M. C. & Prince, S. M. (2013). *Acta Cryst.* **D69**, 1260–1273.
- Zhang, W., Brooun, A., McCandless, J., Banda, P. & Alam, M. (1996). *Proc. Natl Acad. Sci. USA*, **93**, 4649–4654.
- Zhu, X., Amsler, C. D., Volz, K. & Matsumura, P. (1996). *J. Bacteriol.* **178**, 4208–4215.
- Zschiedrich, C. P., Keidel, V. & Surmant, H. (2016). *J. Mol. Biol.* **428**, 3752–3775.